Top-Seeded Solution Crystal Growth and Functional Properties of a Polar Material—Na 2 TeW 2 O 9

ARTICLE *in* CRYSTAL GROWTH & DESIGN · SEPTEMBER 2010

Impact Factor: 4.89 · DOI: 10.1021/cg100762b

4 AUTHORS, INCLUDING:

Weiguo Zhang
University of Houston
26 PUBLICATIONS **354** CITATIONS
SEE PROFILE

Sang-Hwan Kim
University of Houston
30 PUBLICATIONS **534** CITATIONS
SEE PROFILE

Shiv Halasyamani
University of Houston
266 PUBLICATIONS **5,768** CITATIONS
SEE PROFILE

DOI: 10.1021/cg100762b

CRYSTAL GROWTH & DESIGN Article

2010, Vol. 10
4091–4095

Top-Seeded Solution Crystal Growth and Functional Properties of a Polar Material—$Na_2TeW_2O_9$

Weiguo Zhang, Feng Li,[†] Sang-Hwan Kim, and P. Shiv Halasyamani*

Department of Chemistry, University of Houston, 136 Fleming Building, Houston, Texas 77204-5003.
[†]Current Address: Xinjiang Technical Institute of Physics & Chemistry, Chinese Academy of Sciences, 40-1 South Beijing Road, Urumqi 830011, China.

Received June 7, 2010; Revised Manuscript Received July 3, 2010

ABSTRACT: Centimeter-size single crystals of the noncentrosymmetric and polar material $Na_2TeW_2O_9$ were successfully grown through a top-seeded solution growth (TSSG) method. Differently oriented seeds, along the [100], [010], and [001] directions, were used to grow large single crystals. The morphologies of the grown crystals with different oriented seeds are described. $Na_2TeW_2O_9$ crystallizes in the noncentrosymmetric and polar monoclinic space group *Ia* (No. 9). Functional properties including piezoelectricity and polarization were also measured. The d_{11} and d_{33} piezoelectric coefficients are 4.0 pC/N and 13.9 pC/N, respectively. Polarization measurements indicate that although $Na_2TeW_2O_9$ is polar, the material is not ferroelectric; that is, the polarization is not switchable. In addition, optical measurements indicate a UV absorption edge near 360 nm, with a transmission window up to 5 μm.

Introduction

Noncentrosymmetric (NCS) and polar materials are of current interest, owing to their important functional properties, such as pyroelectricity, piezoelectricity, ferroelectricity, as well as second-order nonlinear optical phenomena.[1−6] Many strategies have been described to increase the incidence of crystallographic NCS in any new material—inorganic and organic.[7−15] We have focused on synthesizing new NCS oxides[16−26] containing cations susceptible to second-order Jahn−Teller (SOJT) distortions[27−34]—octahedrally coordinated d^0 transition metals (Ti^{4+}, Nb^{5+}, Mo^{6+}, W^{6+}, V^{5+}, etc.) and lone-pair cations (Se^{4+}, Te^{4+}, Pb^{2+}, etc.). Attributable to SOJT effects, these cations are in locally polar coordination environments. With the octahedrally coordinated d^0 transition metals, the cation is often found displaced from the center of its oxide octahedron toward a corner, face, or edge, whereas with the lone-pair cation a stereoactive lone-pair is observed that results in a highly asymmetric coordination environment. Polar materials that contain these cations that we have synthesized include $BaTeMo_2O_9$,[19] $BaTeW_2O_9$,[19] $Na_2Te_3Mo_3O_{16}$,[20] $Na_2TeW_2O_9$,[16] $Cs_2TeW_3O_{12}$,[18] and $Rb_2TeW_3O_{12}$.[18] In each of these compounds, the local polarizations constructively add, resulting in a macroscopically polar material. In order to fully understand the relationship between the crystal structure and the functional properties, large single crystals are often needed. Recently, large single crystals of $BaTeMo_2O_9$ were grown successfully, and important functional physical properties were reported.[35−38]

We report the crystal growth of $Na_2TeW_2O_9$,[16] a polar material that crystallizes in space group *Ia*, through a top seeded solution growth (TSSG) method. The large single crystals were grown using seeds oriented along the [100], [010], and [001] directions. In addition to the crystal growth, we investigate the crystal morphology with respect to seed orientation, as well as report on the optical spectra, piezoelectricity, and polarization. Structure−property relationships are also discussed.

*Corresponding author e-mail address: psh@uh.edu.

Experimental Section

Synthesis. A large quantity of polycrystalline $Na_2TeW_2O_9$ was synthesized by solid-state reaction techniques. Stoichiometric amounts of Na_2CO_3 (Alfa Aesar, 99.5%), 10.56 g (9.96×10^{-2} mol), TeO_2 (GFS, 99.5%), 15.95 g (9.99×10^{-2} mol), and WO_3 (Alfa Aesar, 99.8%), 46.38 g (2.00×10^{-1} mol), were thoroughly ground and heated in air to 450 °C for 24 h, 500 °C for 24 h, and 600 °C for 72 h with intermittent regrindings. The resultant white powder was found to be pure $Na_2TeW_2O_9$ by powder X-ray diffraction.

Single Crystal Growth of $Na_2TeW_2O_9$. Single crystals of $Na_2TeW_2O_9$ were grown by the top seeded solution growth (TSSG) method using differently oriented seeds. The seeds of $Na_2TeW_2O_9$ were selected from the spontaneous nucleation crystals. The saturation temperature was determined by observing the growth or dissolution of the seed crystals when soaking in the melt. Polycrystalline $Na_2TeW_2O_9$ was mixed with TeO_2 at the molar ratio $Na_2TeW_2O_9/TeO_2$ = 1:0.4, and the mixture was heated up to 700 °C in a platinum crucible in a vertical furnace equipped with a Pt−Rh/Pt thermocouple with a Al-808P controller. The temperature was held for 24 h in order to form a homogeneous melt. Another manner in which to obtain a homogeneous melt is to heat Na_2CO_3, TeO_2, and WO_3, at the molar ratio 1:1.4:2, to 630 °C and hold for 20 h. After 20 h, the mixture should be heated to 700 °C to ensure homogeneity. Our results indicate the different preparations had no impact on the crystal growth. An oriented seed was introduced into the melt with a rotation rate of 10 rpm at 5 °C higher than the saturation temperature, followed by decreasing the temperature to the saturation point in 15 min. From the saturation temperature, the melt was cooled at a rate of 0.5 °C per day to about 2 °C below the saturation temperature. A single crystal was hung above the melt surface and cooled slowly to room temperature. Single crystals grown along the [100], [010], and [001] orientations were obtained using the same procedure described above.

Powder Diffraction. Powder X-ray diffraction measurements on polycrystalline $Na_2TeW_2O_9$ were carried out with a PANalytical X'Pert PRO diffractometer equipped with Cu Kα radiation (λ = 1.54056 Å) in the 2θ range from 10° to 70°. The experimental and calculated patterns are in good agreement.

Differential Scanning Calorimetry. Differential scanning calorimetry (DSC) measurements were performed on an EXSTAR 6000 thermal analysis system (model DSC6300). A 15.0 mg polycrystalline sample of $Na_2TeW_2O_9$ was placed in a platinum pan and heated or cooled at a rate of 10 °C min^{-1} between 20 and 750 °C under N_2.

Published on Web 07/21/2010

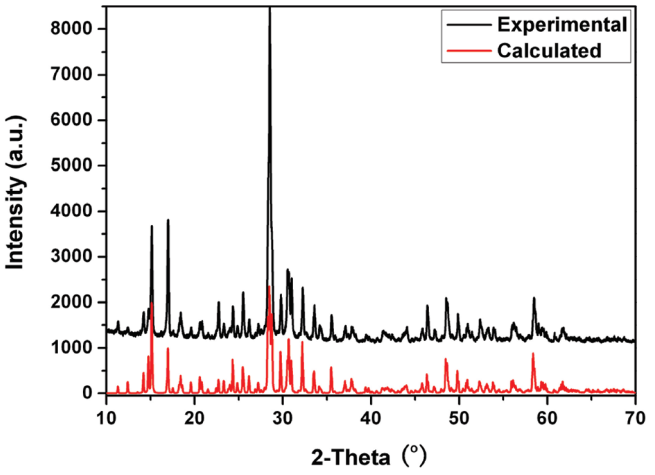

Figure 1. Calculated and experimental powder X-ray diffraction patterns for $Na_2TeW_2O_9$.

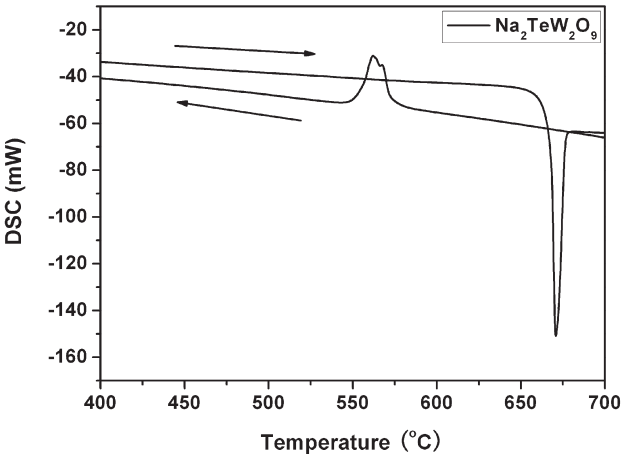

Figure 2. Differential scanning calorimetry data for $Na_2TeW_2O_9$. Note that there is one endothermic peak upon heating (~670 °C) and two exothermic peaks during cooling (~568 °C and ~562 °C), indicating $Na_2TeW_2O_9$ melts incongruently.

After the DSC measurement, powder X-ray diffraction was taken of the residue in the platinum pan.

Optical Spectra Measurement. UV−visible reflectance data were collected on a Varian Cary 500 scan UV−vis−NIR spectrophotometer over the 200−1500 nm spectral range at room temperature. A small piece of the single crystal was ground into fine powder and poly tetrafluoroethylene was used as a reference material. The reflectance spectrum was converted to absorbance using the Kubelka−Munk function.[39,40] Infrared transmission spectra were recorded on a Matteson FTIR 5000 spectrometer in the 400−4000 cm^{-1} range.

Piezoelectric Measurements. Direct piezoelectric data were collected on a YE2730A d_{33} meter (APC International, Ltd.). According to the IEEE standard,[41] *X*-cut and *Z*-cut samples were cut from $Na_2TeW_2O_9$ single crystals with sizes of 3.0 mm (width) × 6.5 mm (length) × 1.0 mm (thickness) and 3.0 mm (width) × 7.5 mm (length) × 1.0 mm (thickness), respectively. The Cartesian coordinates with respect to the crystallographic coordinates are shown in Figure S5 (see Supporting Information). In addition, converse piezoelectric measurements were performed using a Radiant Technologies RT66A piezoelectric test system with a TREK (model 609 × 10^{-6}) high-voltage amplifier, Precision Materials Analyzer, Precision High-Voltage Interface, and MTI 2000 Fotonic Sensor. For the converse piezoelectric measurements, each sample was covered by silver paste on both sides as electrodes and cured at 300 °C for 3 h. The applied voltages for *X*-cut and *Z*-cut samples were 1100 V and 900 V, respectively.

Polarization Measurements. The *Z*-cut sample crystal used in the piezoelectric measurements was used in the polarization measurements. The polarization was measured on a Radiant Technologies RT66A Ferroelectric Test System with a TREK high voltage amplifier between 40 and 160 °C in 20 °C increments in a Delta 9023 environmental test chamber. The temperature was allowed to stabilize before the polarization was measured. The unclamped pyroelectric coefficient, defined as dP/dT (change in the polarization with respect to the change in temperature), was determined by measuring the polarization as a function of temperature. A detailed description of the methodology used has been published elsewhere.[42] To determine the ferroelectric behavior, the polarization loop was measured at room temperature under a static electric field of 8−16 kV/cm in the 50−1000 Hz frequency range.

Results and Discussion

Synthesis and Characterization of $Na_2TeW_2O_9$. Polycrystalline $Na_2TeW_2O_9$ was synthesized by solid state reaction techniques. The powder X-ray diffraction patterns of $Na_2TeW_2O_9$ are in good agreement with the calculated pattern derived from the single crystal data.[16] Figure 1 shows the experimental and calculated powder XRD patterns of the polycrystalline $Na_2TeW_2O_9$. It has been reported that $Na_2TeW_2O_9$ volatilizes above 800 °C;[16] thus, DSC measurements were performed with a maximum temperature of 750 °C. As seen in Figure 2, there is a very sharp endothermic peak around 670 °C, indicating a potentially homogeneous melt. During the cooling process, however, two exothermic peaks around 568 and 562 °C were observed. Powder XRD data on the residue in the platinum pan indicated that $Na_2TeW_2O_9$ decomposed to $Na_2W_2O_7$ and another unknown phase (see Supporting Information Figure S1), indicating that $Na_2TeW_2O_9$ melts incongruently. A TSSG method has to be used to grow large crystals attributable to the incongruent melting of $Na_2TeW_2O_9$.

Growth and Morphologies of the $Na_2TeW_2O_9$ Crystal. Well-shaped faceted yellow single crystals of $Na_2TeW_2O_9$ were grown by the TSSG method using seeds oriented along the [100], [010], and [001] directions. The weights and sizes of the single crystals grown from the seeds are 1.219(2) g, 15 mm × 5 mm × 3 mm − [100] seed, 2.773(4) g, 17 mm × 10 mm × 5 mm − [010] seed, 1.403(5) g, 16 mm × 5 mm × 4 mm − [001] seed. Figure 3 shows the as-grown crystals and simulated morphologies with indexed (*hkl*) planes. As shown in Figure 3, all the different oriented crystals exhibit (110), (101), (−101), and (001) planes. We deduced from the crystal shapes that the highest growth rate is clearly along the [010] direction regardless of the orientation of the seed. There are still many differences among the single crystals when utilizing differently oriented seeds, even though the growth conditions are the same. The crystal grown using the [100] oriented seed has a very regular shape, close to parallelepiped, but with two nonparallel end-faces, whereas the most irregular shaped crystal is found using the [001] oriented seed. The single crystal with the most regular shape was grown using the [010] oriented seed, consistent with the fastest growth direction. Thus, to grow the highest quality and most regular shaped crystal, a [010] oriented seed should be used.

Optical Spectra Analyses of the $Na_2TeW_2O_9$ Crystal. The UV−vis diffuse reflectance spectra indicate the absorption energy for $Na_2TeW_2O_9$ is approximately 3.45 eV. Absorption (K/S) data were calculated from the Kubelka−Munk function.[40]

$$F(R) = \frac{(1-R)^2}{2R} = \frac{K}{S}$$

where R represents the reflectance, K is the absorption coefficient, and S is the scattering factor. In a K/S versus E (eV) plot, extrapolating the linear part of the rising curve to zero provides

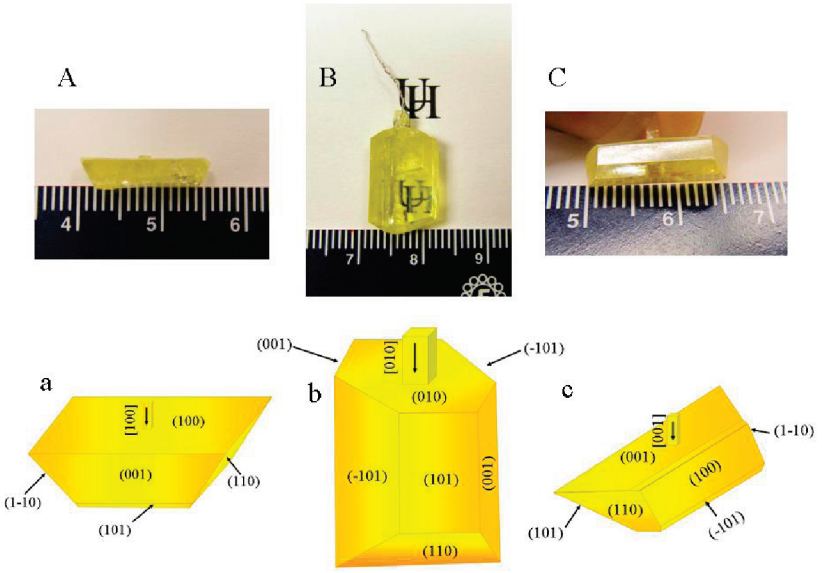

Figure 3. Photos (A−C) and simulated morphologies (a−c) of as-grown $Na_2TeW_2O_9$ single crystals along the [100], [010], and [001] directions. The scale of the ruler is in centimeters.

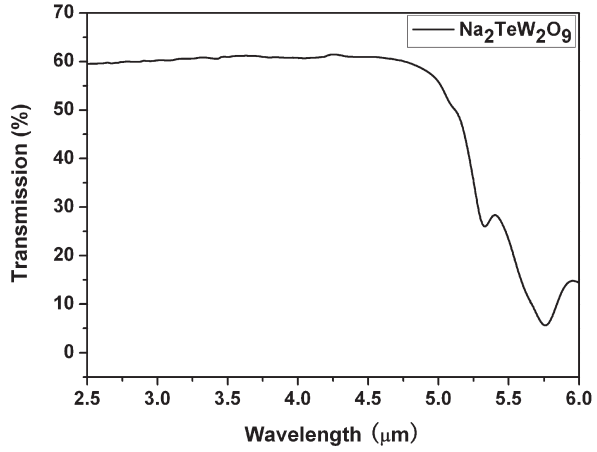

Figure 4. Mid-IR transmission spectra of the $Na_2TeW_2O_9$ crystal perpendicular to the (101) plane. Note that there is good transmission to nearly 5 μm.

the onset of absorption at 3.45 eV (see Supporting Information Figure S2). This indicates the UV absorption edge of the $Na_2TeW_2O_9$ single crystal is around 360 nm. In Figure 4, the infrared transmission spectra of a (101) wafer suggest that a $Na_2TeW_2O_9$ single crystal can transmit up to 5 μm. Taking into consideration UV−vis diffuse reflectance spectra and infrared transmission spectra, a $Na_2TeW_2O_9$ single crystal exhibits a very broad transmission range, 0.36−5.0 μm compared to widely used commercial crystals such as β-BaB_2O_4 (BBO) (0.189−3.5 μm),[43] LiB_3O_5 (LBO) (0.16−2.6 μm),[44] KH_2PO_4 (KDP) (0.176−1.4 μm),[45] and $KTiOPO_4$ (KTP) (0.35−4.5 μm).[46] This indicates $Na_2TeW_2O_9$ is a promising candidate for nonlinear optical applications.

Piezoelectricity of the $Na_2TeW_2O_9$ Crystal. Direct and converse pieozoelectric measurements were performed on *X*-cut and *Z*-cut samples, respectively. The estimated *d* coefficient values are given in Table 1 along with comparable values for SiO_2 and $LiTaO_3$. The piezoelectric data have been deposited in the Supporting Information (see Figures S3 and S4). Although the *d* values determined from the converse method are larger than the values from the direct method,

Table 1. Piezoelectric Coefficients Estimated from the Direct and Inverse Methods

	$Na_2TeW_2O_9$		SiO_2[a]	$LiTaO_3$[a]
piezoelectirc coefficients	dir. (pC/N)	inv. (pm/V)	(pm/V)	(pm/V)
d_{11}	4.0	12.7	−2.31	0
d_{22}	0	0	0	7
d_{33}	13.9	41.1	0	8

[a] From ref 37.

it is reasonably considered that the direct method is more accurate because of exclusion of extrinsic contributions, e.g., electrode effects and the "planeness" of the sample surface that would contribute in the converse method. The large difference between the d_{11} and d_{33} values may be explained by examining the crystal structure of $Na_2TeW_2O_9$. As discussed earlier,[18] acentricity and polarity in $Na_2TeW_2O_9$ are attributable to the distorted WO_6 octahedra and TeO_3 polyhedra. The Na^+ cations retain the charge balance without contributing to the local dipole moments. If we examine the local polarizations, i.e., the W−O and Te−O bonds, we note that the largest component of the macroscopic polarization is along the *Z*-axis as opposed to the *X*-axis (see Supporting Information Figure S5). Thus, it is not surprising that, for the piezoelectric coefficients in $Na_2TeW_2O_9$, the d_{33} value is larger than that of d_{11}.

Polarization Measurements. As discussed above, the polarization along the *Z*-axis is much larger than that along the *X*-axis; thus, polarization measurements were performed on the *Z*-cut sample. The unclamped pyroelectric coefficient was determined by measuring the polarization as a function of temperature at 1000 V at different frequencies between 40 and 160 °C. The polarization vs temperature data, and the temperature and frequency dependence of the pyroelectric coefficient have been deposited in the Supporting Information (see Figures S6 and S7, respectively). The pyroelectric coefficient ranges between 3.75 μC/(m^2 K) (1 kHZ) and 11.3 μC/(m^2 K) (50 Hz) at 40 °C. As the material is polar, ferroelectric measurements were performed to investigate any polarization reversibility. Figure 5 shows the polarization vs electric field at various

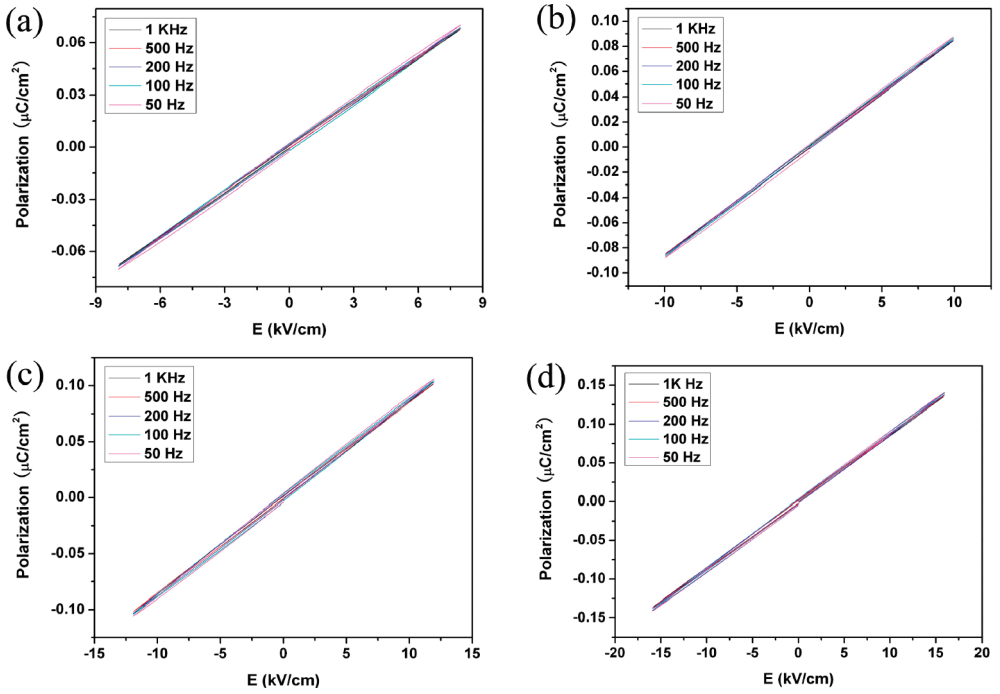

Figure 5. Polarization versus electric field plots at (a) 8 kV/cm, (b) 10 kV/cm, (c) 12 kV/cm, and (d) 16 kV/cm and at different frequencies for a *Z*-cut $Na_2TeW_2O_9$ single crystal. Note that there is no hysteresis, indicating the materials are not ferroelectric, i.e., the polarization is not reversible.

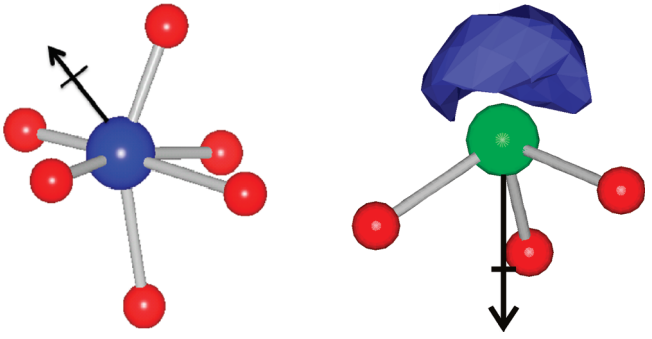

Figure 6. Local oxide coordination of (a) W^{6+} cation (blue) and (b) Te^{4+} cation (green). In both instances, the cation is in a highly asymmetric and polar coordination environment. With part b, visualization of the stereoactive lone-pair through ELF calculations (see Supporting Information) with $\eta = 0.85$ is shown. The figure was made using the program Vesta.[47]

frequencies and voltages. Clearly, a linear relationship between polarization and electric field is observed, indicating that $Na_2TeW_2O_9$ is not ferroelectric. In order for $Na_2TeW_2O_9$ to be ferroelectric, the local polarizations associated with the WO_6 and TeO_3 polyehdra must be reversed. With all of the W^{6+} cations in the material, a C_3 or face-type distortion is observed (see Figure 6a), whereas for the TeO_3 polyhedra a stereoactive lone-pair is observed (see Figure 6b). Although it is feasible to envision the polarization with respect to the W^{6+} cation switching from one face to the opposite, this polarization reversal seems highly unlikely for the Te^{4+} cation. In order to reverse the polarization associated with the TeO_3 polyehdra, a great deal of structural rearrangement and/or metal−oxygen bond breaking and re-forming would have to occur. Any such polarization reversal would be energetically unfavorable. Thus, polarization associated with $Na_2TeW_2O_9$ is frozen, and the material is not ferroelectric.

Conclusions

We have grown large, several millimeter size, single crystals of $Na_2TeW_2O_9$ through a top-seeded solution growth method. The crystals were grown using seeds oriented along the [100], [001], and [001] directions. Although large single crystals were grown with all three seeds, the most regularly shaped crystal was grown from the [010] seed. Finally, although $Na_2TeW_2O_9$ is polar, the macroscopic polarization is not reversible, indicating the material is not ferroelectric. We are in the process of growing large crystals of other functional materials, and we will be reporting on them shortly.

Acknowledgment. We thank the Robert A. Welch Foundation (Grant E-1457), the ACS PRF 47345-AC10, and the NSF (DMR-0652150) for support. We also thank Prof. Xutang Tao (Shandong University, Jinan, China) for assistance in indexing the *hkl* planes of the $Na_2TeW_2O_9$ single crystals.

Supporting Information Available: Powder XRD pattern, UV-vis diffuse reflectance spectroscopy data, displacement versus electric field plot for the *X*-cut and *Z*-cut of the $Na_2TeW_2O_9$ single crystal, schematic relationship between crystallographic coordinates and cartesian coordinates with respect to the local polarization, spontaneous polarization versus temperature, calculated pyroelectric coefficients, density of states, and visualization of the electron localization function calculations. This material is available free of charge via the Internet at http://pubs.acs.org.

References

(1) Nye, J. F. *Physical Properties of Crystals*; Oxford University Press: Oxford, 1957.
(2) Cady, W. G. *Piezoelectricity: an Introduction to the Theory and Applications of Electromechanical Phenomena in Crystals*; Dover: New York, 1964.
(3) Lang, S. B. *Sourcebook of Pyroelectricity*; Gordon & Breach Science: London, 1974.

(4) Jona, F.; Shirane, G. *Ferroelectric Crystals*; Pergamon Press: Oxford, U.K., 1962.
(5) Waser, R.; Böttger, U.; Tiedke, S. *Polar Oxides: Properties, Characterization, and Imaging*; Wiley-VCH Verlag GmbH & Co. KGaA: Weinheim, 2005.
(6) Marder, S. R.; Sohn, J. E.; Stucky, G. D. *Materials for Non-Linear Optics: Chemical Perspectives*; American Chemical Society: Washington, DC, 1991.
(7) Roy, A.-L.; Chavarot, M.; Rose, E.; Rose-Munch, F.; Attias, A.-J.; Kreher, D.; Fave, J.-L.; Kamierszky, C. *C. R. Chim.* **2005**, *8*, 1256.
(8) Percino, M. J.; Chapela, V. M.; Herrera, A. M.; Gutierrez-Perez, R. *Des. Monomers Polym.* **2000**, *3*, 155.
(9) Kepert, C. J.; Prior, T. J.; Rosseinsky, M. J. *J. Am. Chem. Soc.* **2000**, *122*, 5158.
(10) Maggard, P. A.; Stern, C. L.; Poeppelmeier, K. R. *J. Am. Chem. Soc.* **2001**, *123*, 7742.
(11) Nesterov, V. V.; Antipin, M. Y.; Nesterov, V. N.; Penn, B. G.; Frazier, D. O. *Cryst. Growth Des.* **2004**, *4*, 521.
(12) Mo, X. H.; Ferguson, E.; Hwu, S.-J. *Inorg. Chem.* **2005**, *44*, 3121.
(13) Jiang, H. L.; Huang, S. P.; Fan, Y.; Mao, J. G.; Cheng, W. D. *Chem.—Eur. J.* **2008**, *14*, 1972.
(14) Kong, F.; Jiang, H. L.; Hu, T.; Mao, J. G. *Inorg. Chem.* **2008**, *47*, 10611.
(15) Hu, T.; Qin, L.; Kong, F.; Zhou, Y.; Mao, J. G. *Inorg. Chem.* **2009**, *48*, 2193.
(16) Goodey, J.; Broussard, J.; Halasyamani, P. S. *Chem. Mater.* **2002**, *14*, 3174.
(17) Porter, Y.; Halasyamani, P. S. *J. Solid State Chem.* **2003**, *174*, 441.
(18) Goodey, J.; Ok, K. M.; Broussard, J.; Hofmann, C.; Escobedo, F. V.; Halasyamani, P. S. *J. Solid State Chem.* **2003**, *175*, 3.
(19) Ra, H. -S.; Ok, K. M.; Halasyamani, P. S. *J. Am. Chem. Soc.* **2003**, *125*, 7764.
(20) Chi, E. O.; Ok, K. M.; Porter, Y.; Halasyamani, P. S. *Chem. Mater.* **2006**, *18*, 2070.
(21) Kim, J.-H.; Baek, J.; Halasyamani, P. S. *Chem. Mater.* **2007**, *19*, 5637.
(22) Sivakumar, T.; Chang, H. Y.; Baek, J.; Halasyamani, P. S. *Chem. Mater.* **2007**, *19*, 4710.
(23) Chang, H. Y.; Sivakumar, T.; Ok, K. M.; Halasyamani, P. S. *Inorg. Chem.* **2008**, *47*, 8511.
(24) Yeon, J.; Halasyamani, P. S.; Kityk, I. V. *Mater. Lett.* **2008**, *62*, 1082.
(25) Chang, H. Y.; Kim, S.-H.; Ok, K. M.; Halasyamani, P. S. *Chem. Mater.* **2009**, *21*, 1654.
(26) Kim, S.-H.; Yeon, J.; Halasyamani, P. S. *Chem. Mater.* **2009**, *21*, 5335.
(27) Opik, U.; Pryce, M. H. L. *Proc. R. Soc. London, Ser. A* **1957**, *238*, 425.
(28) Bader, R. F. W. *Mol. Phys.* **1960**, *3*, 137.
(29) Bader, R. F. W. *Can. J. Chem.* **1962**, *40*, 1164.
(30) Pearson, R. G. *J. Am. Chem. Soc.* **1969**, *91*, 4947.
(31) Pearson, R. G. *THEOCHEM* **1983**, *103*, 25.
(32) Wheeler, R. A.; Whangbo, M. H.; Hughbanks, T.; Hoffmann, R.; Burdett, J. K.; Albright, T. A. *J. Am. Chem. Soc.* **1986**, *108*, 2222.
(33) Kunz, M.; Brown, I. D. *J. Solid State Chem.* **1995**, *115*, 395.
(34) Goodenough, J. B. *Annu. Rev. Mater. Sci.* **1998**, *28*, 1.
(35) Zhang, W.; Tao, X.; Zhang, C.; Gao, Z.; Zhang, Y.; Yu, W.; Cheng, X.; Liu, X.; Jiang, M. *Cryst. Growth Des.* **2008**, *8*, 304.
(36) Zhang, W.; Tao, X.; Zhang, C.; Zhang, H.; Jiang, M. *Cryst. Growth Des.* **2009**, *9*, 2633.
(37) Gao, Z.; Tao, X.; Yin, X.; Zhang, W.; Jiang, M. *Appl. Phys. Lett.* **2008**, *93*, 252906.
(38) Gao, Z.; Yin, X.; Zhang, W.; Wang, S.; Jiang, M.; Tao, X. *Appl. Phys. Lett.* **2009**, *95*, 151107.
(39) Tauc, J. *Mater. Res. Bull.* **1970**, *5*, 721.
(40) Kubelka, P.; Munk, F. *Z. Tech. Phys.* **1931**, *12*, 593.
(41) *IEEE Standard on Piezoelectricity*; IEEE Inc.: New York, NY, 1988.
(42) Ok, K. M.; Chi, E. O.; Halasyamani, P. S. *Chem. Soc. Rev.* **2006**, *35*, 710.
(43) Klein, R. S.; Kugel, G. E.; Maillard, A.; Sifi, A.; Polgar, K. *Opt. Mater.* **2003**, *22*, 163.
(44) Chen, C.; Wu, Y.; Jiang, A.; Wu, B.; You, G.; Li, R.; Lin, S. *J. Opt. Soc. Am. B* **1989**, *6*, 616.
(45) Sliker, T. R.; Burlage, S. R. *J. Appl. Phys.* **1963**, *34*, 1837.
(46) Moorthy, S. G.; Kumar, F. J.; Balakumar, S.; Subramanian, C.; Ramasamy, P. *Mater. Sci. Eng. B* **1999**, *60*, 88.
(47) Momma, K.; Izumi, F. VESTA: a three-dimensional visualization system for electronic and structural analysis. *J. Appl. Crystallogr.* **2008**, *41*, 653.